Available online at www.sciencedirect.com
SCIENCE DIRECT®
ELSEVIER
Nuclear Instruments and Methods in Physics Research B 217 (2004) 637–643
NIM B
Beam Interactions with Materials & Atoms
www.elsevier.com/locate/nimb

Sensitivity of LR 115 detectors in hemispherical chambers for radon measurements

D. Nikezic [1], F.M.F. Ng, K.N. Yu *

Department of Physics and Materials Science, City University of Hong Kong, 83 Tat Chee Avenue, Kowloon Tong, Kowloon, Hong Kong

Received 20 August 2003; received in revised form 4 November 2003

Abstract

We have determined the detection sensitivity of the LR 115 detector placed on the bottom of hemispherical diffusion chambers through Monte Carlo simulations. For the cases where the LR 115 detectors completely cover the bottom of hemispherical diffusion chambers, we propose the optimum radius of the hemispherical chamber as 3 cm. In hemispherical chambers with radii smaller than 3 cm, the total sensitivity is smaller which will lower the number of tracks and increase the statistical uncertainty. On the other hand, if the radius is larger than 3 cm, the effects of the deposition fraction of radon progeny will come into effect, which will again introduce uncertainties in radon measurements. For the hemispherical chamber with a radius of 3 cm, we further propose the detector radius to be 1.3 cm. This combination will eliminate the influence of the deposition fraction on the total sensitivity and at the same time give a large total sensitivity. For a detector with this radius, the hemispherical chamber with a radius of 3 cm is the largest one which provides the total sensitivity independent of the deposition fraction of radon progeny.

PACS: 29.40; 23.60
Keywords: Natural radioactivity; Radon; LR 115 detector; Detector sensitivity

1. Introduction

Solid state nuclear track detectors (SSNTDs) have been applied for radon measurements of ^{222}Rn over a relatively long period. They are usually placed inside a cup which is closed with a filter paper or some other permeable materials. Such a system (cup with filter paper) is called the "diffusion chamber" since ^{222}Rn gas diffuses into it. On the other hand, the short-lived progeny of the ^{222}Rn gas, as well as dust and water droplets, are filtered out. In this way, the diffusion chamber is a device measuring radon gas alone. A variety of diffusion chambers have been described in the literature and applied in real-life measurements of radon gas concentrations in air and in soil. The most commonly used diffusion chambers are cylindrical or semi-conical. However, there are also other designs such as the hemispherical one. Existing diffusion chambers with SSNTDs used for

* Corresponding author. Tel.: +852-2788-7812; fax: +852-2788-7830.
E-mail address: peter.yu@cityu.edu.hk (K.N. Yu).
[1] On leave from University of Kragujevac, Serbia and MonteNegro.

0168-583X/$ - see front matter © 2003 Elsevier B.V. All rights reserved.
doi:10.1016/j.nimb.2003.12.040

radon measurements have been reviewed by Khan et al. [1] and Nikolaev and Ilic [2].

The detector sensitivity S to radon is usually expressed by the number of tracks per unit detector surface (track/m^2) obtained under a unit exposure (Bq s/m^3), or just simplified as (m). It depends on a number of factors including the type of SSNTD, etching and readout procedures, geometry of the chamber and SSNTD, as well as environmental parameters such as temperature, pressure, relative humidity, distribution of local electrical fields in and around the chamber. The sensitivity S is usually determined experimentally through exposure of the SSNTD to a known radon concentration for a known period of time [3].

On the other hand, the sensitivity S can also be determined using theoretical models [4–25]. The models listed here are for references only. Comparisons of results from these models are beyond the scope of the present paper. These methods are broadly divided into two categories, namely the analytical approach and the Monte Carlo simulation approach.

Modeling of alpha particle detection by SSNTDs in diffusion chambers will enable better understanding of radon measurements by the method. The following tasks are also made possible:

- investigation of the effects of the shape and dimensions of the chamber and the detector on the sensitivity;
- calculations of the contribution of particular alpha emitters (radon or radon progeny) to the total sensitivity;
- examination of the consequence of progeny deposition onto inner chamber walls;
- calculation of track density distribution and relating it to the deposition pattern of radon progeny, etc.

Most of the previously mentioned works deal with the cylindrical or semi-conical diffusion chambers. These two geometries are the most studied and most often used for radon measurements. Other geometries of the chamber are less studied. For example, the rectangular geometry was considered theoretically only in one paper [13].

The hemispherical chamber was previously described and theoretically studied by Urban [8]. The Makrofol detector covered with an alluminized mylar foil was used in this chamber, with subsequent electrochemical etching after exposure. The authors claimed that this system might be used for simultaneous measurements of radon, thoron and their progeny. The measurements were based on comparisons between the measured track size distribution and the theoretically predicted distribution for various exposure situations. If filtering is applied, the device is used only for radon measurements.

In this paper, we simulate the response of the LR 115 detector in hemispherical diffusion chambers. The objective is to investigate the potential of such chambers for radon measurements with this kind of detector. It is convenient to cut the LR 115 detector in any form. For example, the circular shape adopted for this work can be created easily. In Fig. 1, a hemispherical diffusion chamber with a detector placed on the base is schematically presented. This scheme is similar to the one depicted by Urban [8].

One difficult problem in using diffusion chambers with SSNTDs to measure radon gas concentrations is due to the influence of the deposition fraction of short lived radon progeny [21,22]. After radon gas diffuses into a diffusion chamber, radon progeny will be formed. A fraction of the progeny decays before deposition onto available inner surfaces of the chamber, and the rest is the deposition fraction which decays after deposition. From the results obtained in the present study, we hope to be able to give optimized size of the diffusion chamber and the size of the LR 115 detec-

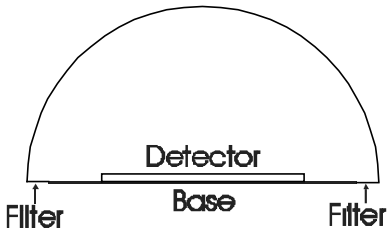

Fig. 1. The schematic diagram showing a hemispherical diffusion chamber for radon measurements, which is equipped with a detector on the bottom.

tor, which provides the largest sensitivity while minimizing the influence of the deposition fraction.

2. Simulation method

Previously described programs based on the Monte Carlo method [10,11] were used to simulate the propagation of alpha particles in air and their detection by the LR 115 detector, and the corresponding description will not be repeated here in details. The concept of the effective volume defined earlier is employed in this work. However, the effective volumes for all alpha energies are recalculated because of some modifications in the calculation model. These modifications are made to improve the accuracy of the program, and have been introduced in two main areas of the model. The first one concerns calculations of stopping powers and ranges of alpha particles in air and in cellulose nitrate. In earlier versions of our programs, calculations of the stopping powers in air and in cellulose nitrate made use of the Bethe–Bloch's expression, which is now replaced by the SRIM code [26]. Our task is to calculate the energy E_x of an alpha particle with initial energy E_0 after traveling a distance x in air. The table produced by the SRIM code gives the stopping power as a function of the alpha particle energy. These data have been fitted by a standard fitting procedure provided by the SigmPlot® software, and a function $S = f(E)$ has been obtained. The energy E_x of the alpha particle is determined by the integral

$$x = \int_{E_x}^{E_0} \frac{\mathrm{d}E}{f(E)}. \tag{1}$$

An iteration procedure has to be invoked here because the unknown quantity is the lower bound of the integral (the known quantities in the course of the Monte Carlo simulations are E_0 and x, the latter being the distance between the emission point of the alpha particle and the point where it enters the detector).

The ranges of alpha particles in the LR 115 detector are also determined using the data obtained from the SRIM program. Since the energy of the alpha particles incident on the detector can be any value from 0 to E_0, the corresponding range may have to be determined through linear interpolations between the data given by SRIM.

The second important modification in the program concerns the determination of the track parameters. The models of Somogyi and Szalay [27] and Nikezic and Kostic [28] for the track growth were used in earlier versions of our programs, which are now replaced by the model recently developed by Nikezic and Yu [29].

To simulate formation of tracks in the LR 115 detector from alpha particles and to calculate the track parameters, one needs to know the track etch rate V_t and bulk etch rate V_b. The bulk etch rate of the LR 115 detector have been measured by many authors [4,30–35] giving values between about 2 and 7 $\mu m\,h^{-1}$. In this work, we adopt $V_b = 3.27$ $\mu m\,h^{-1}$ determined previously from direct surface profilometry measurements of Type 2 non-strippable LR 115 films from DOSIRAD, France [32]. This bulk etch rate was determined under standard etching conditions for this detector: 2.5 N aqueous solution of NaOH at 60 °C without stirring. Assuming that the etching lasts for 2 h, the thickness of the removed active layer will be 6.54 μm. By adopting the initial thickness 12 μm of the LR 115 detector as quoted by the manufacturer (DOSIRAD, France) (see also discussion in [34]), the thickness of the remaining active layer should be 5.46 μm.

In contrast to V_b, information on the track etch rate V_t for alpha particles in LR 115 is relatively scarce. We adopt the V function ($= V_t/V_b$) published by Durrani and Green [36] as

$$V = 1 + (100\mathrm{e}^{-0.446R'} + 5\mathrm{e}^{-0.107R'})(1 - \mathrm{e}^{-R'}). \tag{2}$$

The particle track length L in the detector is calculated by

$$L = \int_0^T V_t\,\mathrm{d}t - V_b T, \tag{3}$$

where T is the total etching time. If the etchant reaches the end point of the particle track before etching is completed, track etching will progress with the rate V_b in all directions for the rest of the etching time. Tracks whose growths do not start at the initial detector surface are also considered.

In the calculations, we have adopted the following two criteria, both of which should be met for the observation of tracks: (i) the tracks perforate completely the active layer of the detector and (ii) the track diameter is larger than 1 μm.

3. Results and discussion

Calculations have been performed for alpha particles with energies in the ^{222}Rn chain, namely, 5.49 MeV for ^{222}Rn, 6 MeV for ^{218}Po and 7.69 MeV for ^{214}Po(Bi). As mentioned before, the radon progeny can partially decay in air and partially deposit onto the chamber wall before decaying, so both situations are considered here. The results are shown in Figs. 2–5, where the indices (air) and (wall) refer to the progeny being emitted from air and from the chamber wall, respectively.

In Fig. 2, the results for partial sensitivities (in m) for radon and progeny are given. From the partial sensitivity of the LR 115 detector to an airborne radionuclide, we know the track density (in tracks/m^2) obtained per unit exposure (Bq s m^{-3}) of the detector to that radionuclide. It is assumed in the present calculations that the detector covers entirely the base of the chamber, i.e. the air inlet has a negligible width and the radius of the chamber is equal to the radius of cir-

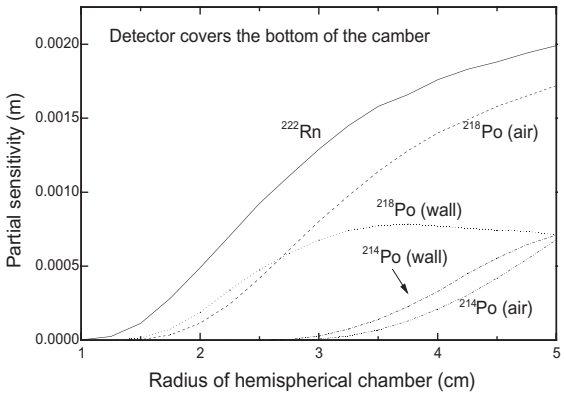

Fig. 2. Partial sensitivities of LR 115 detectors inside hemispherical chambers to radon and its progeny. The detectors cover the bottom of the chambers.

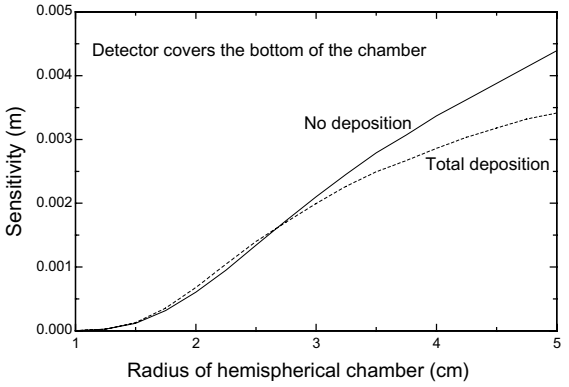

Fig. 3. Total sensitivities of LR 115 detectors in hemispherical chambers to radon and its progeny. The detectors cover the bottom of the chambers.

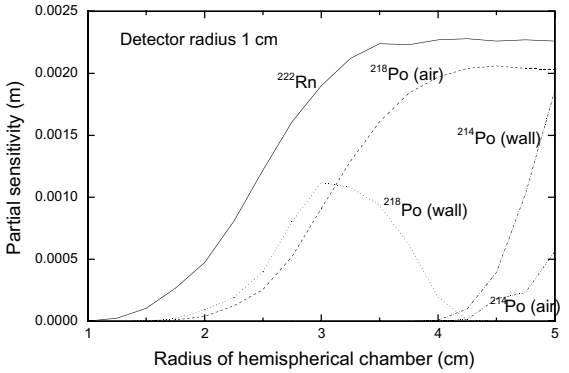

Fig. 4. Partial sensitivities of LR 115 detectors in hemispherical chambers to radon and its progeny. Detector radius is 1 cm.

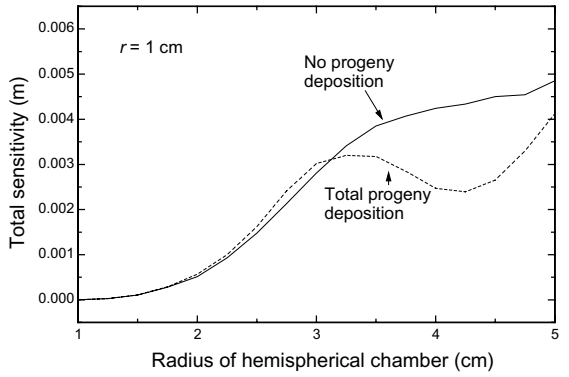

Fig. 5. Total sensitivities of LR 115 detectors in hemispherical chambers to radon and its progeny. Detector radius is 1 cm.

cular detector. There are five curves in the graph shown in Fig. 2. In general, the partial sensitivities increase with the chamber radius. All the curves tend to saturate beyond some radii. However, most of these radii are so large that diffusion chambers with these radii will not have practical applications, so only the results for radii up to 5 cm will be presented.

The largest sensitivities are for ^{222}Rn; its alpha energy, 5.49 MeV, is the closest to the upper energy threshold (4.6 MeV) of the LR 115 detector. The curve for ^{218}Po is below that for ^{222}Rn, with the smaller sensitivity being attributed to the higher energy of the alpha particles. These two curves are almost parallel because their energies are not very different from each other. The curve for ^{214}Po is far below the previous two because its alpha energy is much higher. It is noted that the detector will not record any alpha particles emitted by ^{214}Po if the radius of the chamber is smaller than 2.5 cm. Alpha particles with an initial energy of 7.69 MeV emitted from the wall and from the air volume have almost the same chance to generate tracks in the LR 115 detector, so the curves for ^{214}Po (air) and ^{214}Po (wall) are close to each other. Finally, the sensitivity for ^{218}Po (wall) achieves maximum for a chamber with radius of about 3.5 cm and drops slightly for larger chambers.

Furthermore, the total sensitivities have been calculated for two extreme cases: (a) all radon progeny decay in air before deposition and (b) all radon progeny decay after deposition on the wall, where uniform deposition is assumed on all internal surfaces of the chamber. The curves for these two extreme cases are given in Fig. 3. The two curves are very close to each other for diffusion chambers with radii up to 3 cm. Apparently, there are some self-compensating effects in the chamber. This means that the detector response does not depend on the deposition behavior of radon progeny inside a spherical chamber if $R < 3$ cm. Even for chambers with radii larger than 3 cm, the differences between two curves are not too large. For example, for a chamber with a radius of 5 cm, the uncertainty is less than 13%. In contrast, for cylindrical diffusion chambers with radii larger than 3 cm, the unknown fraction of deposited ^{218}Po can cause an uncertainty up to 30% in radon measurements.

In the discussions above, when the radius of the diffusion chamber changes, the radius of the detector changes accordingly since the detector has been designed to cover completely the base of the diffusion chamber. In the following, we will consider the cases where the size of the detector has been fixed to have a radius r of 1 cm. The results for the partial sensitivities and the total sensitivities are shown in Figs. 4 and 5, respectively.

4. Influence of detector size on sensitivity

As shown in [37–39], the track density on detectors placed on the bottom of cylindrical chambers is not uniform and varies with the distance from the center of the detector. The non-uniform track density in fact implies the dependence of the total sensitivity on the detector size.

The effect of the detector size on the total sensitivity has not been widely studied in the past, neither experimentally nor theoretically. Here, we have varied the detector radius in the hemispherical chamber and calculated the total sensitivity in order to gain some ideas about this dependence.

Calculations have been performed for hemispherical chambers with radii of 2, 3 and 4 cm. The detector radius was varied from 1 cm up to the chamber radius and the results are shown in Fig. 6. The solid lines were obtained for the case where all radon progeny decay in air before deposition and the dashed lines for the case where all radon progeny decay after deposition on the wall.

For the chamber with radius $R = 2$ cm, the dependence of the total sensitivity on the detector radius is weak. Furthermore, as the solid line and the dashed line for this chamber are close, the sensitivity only weakly depends on the deposition fraction of radon progeny regardless of the size of the detector, which is a desirable feature for diffusion chambers. However, the total sensitivity in this small chamber is very low.

For the chamber with radius $R = 3$ cm, the total sensitivities are larger than those for the chamber with $R = 2$ cm by factors from 3 to 5. However, for the chamber with radius $R = 3$ cm, the sensitivity

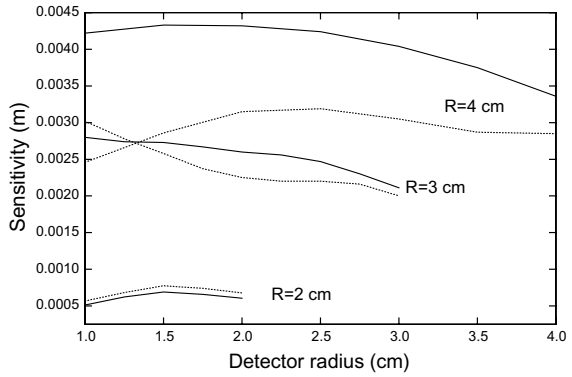

Fig. 6. Dependence of the total sensitivity on the detector radius for different hemispherical chambers with radii $R = 2$, 3 and 4 cm. The solid lines were obtained for the case where all radon progeny decay in air before deposition and the dotted lines for the case where all radon progeny decay after deposition on the wall.

is dependent of the deposition fraction. From the results in Section 3, we know that when the radius of the detector is equal to the radius of the chamber, i.e. 3 cm, the sensitivity is essentially independent on the deposition fraction. When the detector gets smaller, the solid line and the dashed line get farther apart initially, but then get close together again. An interesting point is at the detector radius of $r = 1.3$ cm where the solid and the dashed curves intersect, which means no dependence on the deposition fraction at this detector radius. If we would like to eliminate the uncertainties due to the unknown deposition fraction of radon progeny, we can choose a detector of this size. Furthermore, the total sensitivity for the detector with this size ($r = 1.3$ cm) is higher than that for the detector with $r = 3$ cm.

The largest examined chamber with $R = 4$ cm has the largest sensitivity, but the solid and the dashed curves are far from each other and do not intersect.

5. Conclusions

In this paper, we have determined the detection sensitivity of the LR 115 detector placed on the bottom of hemispherical diffusion chambers through Monte Carlo simulations. In chambers with radii smaller than 3 cm, the detectors with the same radius as that of the diffusion chamber will have sensitivities independent of the deposition fraction of radon progeny. These combinations of diffusion chambers and detectors can thus provide reproducible and stable results in radon measurements, which are independent of environmental conditions that may alter the deposition behavior of radon progeny.

We therefore propose the optimum radius of the hemispherical chamber as 3 cm. In hemispherical chambers with radii smaller than 3 cm, the total sensitivity is smaller which will lower the number of tracks and increase the statistical uncertainty. On the other hand, if the radius is larger than 3 cm, the effects of the deposition fraction of radon progeny will come into effect, which will again introduce uncertainties in radon measurements. For the hemispherical chamber with a radius of 3 cm, we further propose the detector radius r to be 1.3 cm. At this detector radius, the total sensitivities for the case where all radon progeny decay in air before deposition and for the case where all radon progeny decay after deposition on the wall are the same. In Fig. 7, the total sensitivities of the detector with this radius for hemispherical chambers with different radii are shown, which shows that the hemispherical chamber with a radius of 3 cm is the largest one

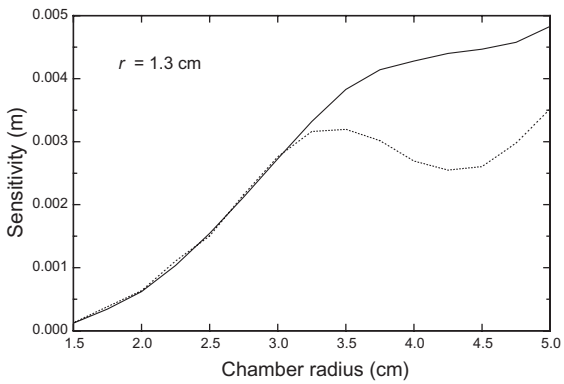

Fig. 7. Sensitivity for the detector with a radius of 1.3 cm in hemispherical chambers with different radii. The solid line was obtained for the case where all radon progeny decay in air before deposition and the dotted line for the case where all radon progeny decay after deposition on the wall.

which provides a total sensitivity independent of the deposition fraction of radon progeny.

Acknowledgements

The present research is supported by the CERG grant CityU1081/01P from the Research Grant Council of Hong Kong (City University of Hong Kong reference number 9040639).

References

[1] H.A. Khan, I.E. Qureshi, M. Tufail, Radiat. Prot. Dosim. 46 (1993) 149.
[2] V.A. Nikolaev, R. Ilic, Radiat. Meas. 34 (2001) 181.
[3] J.C.H. Miles, in: S.A. Durrani, R. Ilic (Eds.), Radon Measurements by Etched Track Detectors. Application to Radiation Protection, Earth Sciences and Environment, World Scientific, Singapore, 1997, p. 143.
[4] N. Nakahara, H. Kudo, F. Akiba, Y. Murakami, Nucl. Instr. and Meth. 171 (1980) 171.
[5] A. Sadig, A. Waheed, E.U. Khan, H.A. Khan, R.A. Akber, in: P.H. Fowler, V.M. Clapham (Eds.), Proc. 11th Int. Conf. on Solid State Nuclear Tracks Detectors, Bristol, Pergamon Press, Oxford, 1981, p. 543.
[6] G. Somogyi, S. Paripas, Zs. Varga, Nucl. Tracks Radiat. Meas. 8 (1984) 423.
[7] A. Demkjaer, Nucl. Tracks 12 (1986) 295.
[8] M. Urban, Nucl. Tracks 12 (1986) 685.
[9] L.E. Qureshi, M. Tufail, H. Saleem, H.A. Khan, Nucl. Tracks. Radiat. Meas. 19 (1–4) (1991) 385.
[10] D. Nikezic, P. Markovic, Dj. Bek Uzarov, Health Phys. 62 (1992) 239.
[11] D. Nikezic, P. Markovic, Dj. Bek Uzarov, Health Phys. 64 (1993) 628.
[12] S. Djeffal, M. Allab, Radiat. Prot. Dosim. 47 (1993) 611.
[13] S.M. Mirza, N.M. Mirza, M. Tufail, N. Ahmad, Radiat. Prot. Dosim. 46 (1993) 15.
[14] R. Andriamanantena, W. Enge, Radiat. Meas. 25 (1995) 625.
[15] O. Sima, Radiat. Meas. 25 (1995) 603.
[16] R. Andriamanatena, G.U. Bacmeister, K. Freyer, R. Ghose, G. Jonsson, T. Kleis, H.C. Treutler, W. Enge, Radiat. Meas. 28 (1997) 657.
[17] D. Nikezic, K.N. Yu, Nucl. Instr. and Meth. A 419 (1998) 175.
[18] D. Pressyanov, I. Rusinov, G. Simeonov, Nucl. Instr. and Meth. A 435 (1999) 509.
[19] R. Barillon, A. Chambaudet, J. Radioanal. Nucl. Chem. 243 (2000) 607.
[20] M.A. Misdaq, H. Khajmi, F. Aitnouh, S. Berrazzouk, W. Bourzik, Nucl. Instr. and Meth. B 171 (2000) 350.
[21] D. Nikezic, K.N. Yu, Health Phys. 78 (2000) 414.
[22] D. Nikezic, K.N. Yu, Nucl. Instr. and Meth. A 450 (2000) 568.
[23] F. Bagnoli, F. Bochicchio, S. Bucci, D. Marocco, Radiat. Meas. 34 (2001) 207.
[24] O. Sima, Radiat. Meas. 34 (2001) 181.
[25] F.U. Rehman, K. Jamil, M. Zakaullah, F. Abu-Jarad, S.A. Mujahid, J. Environ. Radioact. 65 (2003) 243.
[26] J.F. Ziegler, SRIM-2000, 2001. http://www.srim.org/.
[27] G. Somogyi, A.S. Szalay, Nucl. Instr. and Meth. 109 (1973) 211.
[28] D. Nikezic, D. Kostic, Radiat. Meas. 28 (1997) 185.
[29] D. Nikezic, K.N. Yu, Radiat. Meas. 37 (2003) 39.
[30] G. Somogyi, I. Hunyadi, Zs. Varga, Nucl. Track Detection 2 (1978) 191.
[31] S. Sanzelle, J. Fain, D. Mialler, Nucl. Tracks 12 (1986) 913.
[32] D. Nikezic, A. Janicijevic, Appl. Radiat. Isot. 57 (2002) 275.
[33] J.P.Y. Ho, C.W.Y. Yip, V.S.Y. Koo, D. Nikezic, K.N. Yu, Radiat. Meas. 35 (2002) 571.
[34] C.W.Y. Yip, J.P.Y. Ho, V.S.Y. Koo, D. Nikezic, K.N. Yu, Radiat. Meas. 37 (2003) 197.
[35] C.W.Y. Yip, J.P.Y. Ho, D. Nikezic, K.N. Yu, Radiat. Meas. 36 (2003) 161.
[36] S.A. Durrani, P.F. Green, Nucl. Tracks 8 (1984) 21.
[37] D. Nikezic, K.N. Yu, Nucl. Instr. and Meth. A 437 (1999) 531.
[38] V.S.Y. Koo, C.W.Y. Yip, J.P.Y. Ho, D. Nikezic, K.N. Yu, Nucl. Instr. and Meth. A 491 (2002) 470.
[39] V.S.Y. Koo, C.W.Y. Yip, J.P.Y. Ho, D. Nikezic, K.N. Yu, Appl. Radiat. Isot. 59 (2003) 49.